Emission in the ion cyclotron range of frequencies (ICE) on NSTX and NSTX-U

E. D. Fredrickson, N. N. Gorelenkov, R. E. Bell, A. Diallo, B. P. LeBlanc, M. Podestà and the NSTX team

Princeton Plasma Physics Laboratory, Princeton New Jersey 08543

eric@pppl.gov

Abstract.

We report here on observations of magnetic fluctuations in the ion-cyclotron frequency range on NSTX and NSTX-U. In many respects the fluctuations appear similar to the ion cyclotron emission (ICE) seen in conventional tokamaks. However a significant difference between previous observations of ICE and the ICE on NSTX is that the frequency of ICE in conventional tokamaks is typically near the ion cyclotron frequency of the energetic fast ions at the plasma edge. In NSTX and NSTX-U the magnetic fluctuation frequency corresponds to the ion cyclotron frequency deeper in the plasma, near the location of an internal transport barrier. As on conventional tokamaks, higher harmonics of the deuterium cyclotron frequency, as high as the seventh, are seen with the strongest signal sometimes from higher harmonics. The emission usually appears as an irregular sequence of short bursts typically $\leq$100 μs in duration, although nearly continuous emission for several ms has also been seen under some conditions. Measurements of the emission with a toroidal array of fast probes find that the emission is a long wavelength, spatially coherent mode. The emission frequency doesn't follow an Alfvénic scaling with density, as seen for compressional Alfvén eigenmodes, but does show a linear scaling with local magnetic field strength. The measured emission shows a compressional polarization consistent with a compressional Alfvén wave. No correlation between neutron rate and ICE amplitude is seen. Three-wave coupling between the instability responsible for the ICE and lower frequency modes has also been observed.

Keywords: ICE, energetic particles, NSTX

1. Introduction

Extensive measurements have been made of super-thermal wave emission in the ion-cyclotron frequency range from laboratory plasmas [1-18]. The emission is commonly referred to as ion cyclotron emission or ICE. For tokamaks, the emission typically has some universal characteristics. The ICE appears as a sequence of narrow peaks at multiples of the edge ion cyclotron frequency of super-thermal ions created by neutral beam injection, radio-frequency heating of a minority ion population, or fusion reactions. Sometimes at higher harmonics a broad continuum of emission is also seen. Where measurements have been made, the ICE tends to have long wavelengths [11]. Under some conditions the amplitude of ICE emission is found to be proportional to the fusion neutron rate, sparking ongoing interest in the possibility of using measurements of ICE to infer characteristics of the confined super-thermal ion population, most importantly those originating from fusion reactions [17-22]. A complete theoretical understanding of ICE is lacking and an improved theoretical

understanding is necessary if ICE is to be used as a diagnostic of confined fast ions. Measurements of ICE on spherical tokamaks, with low magnetic fields and beam energies similar to those on higher field tokamaks provide data from a new parameter regime to test theoretical models for ICE.

Theoretical models based on Alfvén waves [23-30], Ion Bernstein Waves (IBW) [1,2,5,17,20,31] and spin-flip MASER emission from fusion protons [32] have been proposed to explain ICE. The apparent electromagnetic character of the emission has focussed most of the attention on Alfvén wave based models such as the magneto-acoustic cyclotron instability (MCI) or Alfvén Cyclotron Instability (ACI). In these models, compressional Alfvén waves are excited through a Doppler shifted ion cyclotron resonance [23-30]. The models predict that the compressional Alfvén eigenmodes (CAE) would be excited near the plasma edge by an anisotropic fast ion distribution of barely-trapped fusion products or beam ions. The requirement of the resonance means that frequencies should be down-shifted by the parallel motion of the fast ions from the fast-ion cyclotron frequency. The down-shifted ICE frequency would help avoid potentially strong ion-cyclotron damping of the emission by the thermal plasma, but would represent a relatively small shift from the ion cyclotron frequency in tokamaks like TFTR and JET.

Early beam heating experiments on spherical tokamaks saw a broad spectrum of modes [33-40], some of which are identified as Doppler-shifted cyclotron resonance driven CAE [26,38]. The frequency down-shift is relatively larger on spherical tokamaks, which have much lower toroidal fields and cyclotron frequencies than conventional tokamaks but similar beam ion energies. The counter-propagating CAE typically sit at frequencies of order half the edge deuterium ion-cyclotron frequency, consistent with the expected downshift from the co-injected neutral beams. These modes were suggested to be the manifestation of ICE in spherical tokamaks [40,41]. Co-propagating CAE with frequencies up to and exceeding the edge ion-cyclotron frequency were seen on MAST [39] and NSTX [37]. The resonant fast ion drive for co-propagating CAE with frequencies approaching, but below, the edge cyclotron frequency are generally not considered to be through a cyclotron resonance as the Doppler-shifted resonance condition wouldn't be satisfied.

Here we report on observations of a highly coherent instability in the deuterium ion cyclotron frequency range on NSTX [42] and NSTX-U [43]. The pulse length, maximum plasma current, and toroidal field were increased and three neutral beam sources were added in the upgrade from NSTX to NSTX-U. NSTX/NSTX-U is a low aspect ratio tokamak with major radius of ≈ 90 cm, minor radius of ≈ 60 cm. ICE was measured in NSTX plasmas with nominal toroidal field strengths from 2.6 kG up to 4.6 kG. The NSTX-U shots during the commissioning campaign were taken mostly with a toroidal field of 5.9 kG. (Throughout this paper, the toroidal field numbers, unless otherwise noted, refer to the vacuum field at a major radius of 100 cm.) The plasmas were heated with up to 7 MW of neutral beams with

energies up to 100 keV. The ICE is typically seen at low density early in the discharges, often during the current ramps, so the plasma currents ranged from 0.35 MA up to 1.1 MA.

II. Principal observations

In this section we will describe the physical characteristics of the ICE seen on NSTX and NSTX-U, particularly how these observations are similar to, or different from, ICE measurements on conventional aspect ratio tokamaks. The theoretical models for previous observations of ICE interpreted it as an Alfvénic instability [23-30]. Thus, we will also compare the characteristics of the ST-ICE observations to previous studies of compressional Alfvén eigenmodes (CAE) on NSTX and MAST. We will begin with a documentation of the scaling of the ICE frequency with plasma parameters

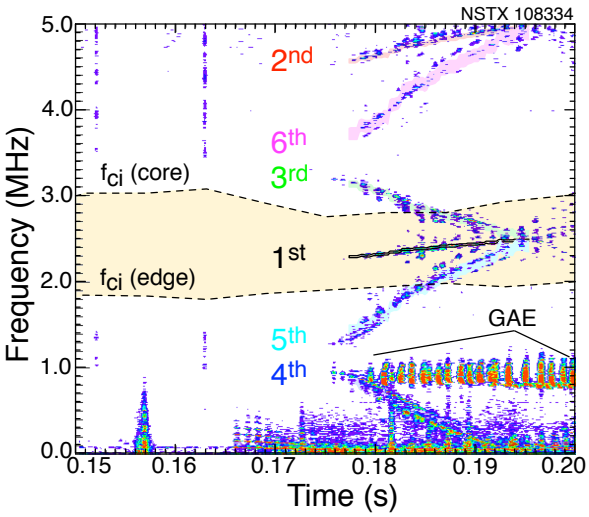

Fig. 1. a) Spectrogram of magnetic fluctuations with the fundamental ICE harmonic in the high-lighted area; frequencies of aliased harmonics indicated by colored bands ($\delta f/f \approx 1\%$). ($I_P \approx 0.8$ MA, $P_{NBI} \approx 1.7$ MW, $B_{tor} \approx 3.4$ kG)

Examples of ICE are shown in Fig. 1 for NSTX and Fig. 2 for NSTX-U. The spectrograms in Figs. 1 and 2 are of magnetic fluctuations measured with a Mirnov coil mounted on the vacuum vessel wall and located approximately 20 cm from the plasma edge. For the NSTX data in Fig. 1, there was only one channel acquired at a 10 MHz sampling rate (although later shots had up to four channels in a toroidal array) and the nominal bandwidth of the detector was ≈1.8 MHz. Most NSTX operation the acquisition rate was reduced to 5 MHz to extend the data acquisition window to accommodate 1 s discharges. The Mirnov coils were re-designed for NSTX-U to extend the bandwidth to ≈ 3 MHz. Above the nominal bandwidth (1.8 MHz or 3 MHz) the Mirnov sensor response falls off approximately inversely with frequency and there are no anti-aliasing filters. For the NSTX-U data shown in Fig. 2 the data acquisition rate was 10 MHz, although there is some data with an acquisition rate of 15 MHz. There are a total of fifteen coils in this array which is configured to measure both poloidal and toroidal magnetic fluctuations, the toroidal mode number of coherent modes, and provide some limited information on the poloidal structure. Eleven coils are arranged in a toroidal array consisting of two groups of three coils and one group of five coils with the groups separated by ≈ 90°. The array is approximately 32 cm above the plasma mid-plane. Eight of these coils are oriented to measure poloidal fluctuations and one coil in each of the three groups is oriented to measure toroidal fluctuations. The remaining four coils, combined with a coil from the toroidal array, make a vertical array spanning ≈ 65 cm centered on the mid-plane.

IIa. ICE frequency higher than edge ion cyclotron frequency.

The ion cyclotron emission seen on NSTX/NSTX-U is similar in many ways to the ICE commonly seen in conventional aspect ratio tokamaks, with some interesting exceptions, and is qualitatively different than the CAE seen on NSTX and MAST. The most significant difference between ICE on conventional tokamaks and ICE on NSTX/NSTX-U is that the ICE frequency is significantly higher than the edge cyclotron frequency. ICE frequencies on conventional tokamaks are typically found to be near harmonics of the cyclotron frequency of the energetic ion species at the outboard plasma edge. The exceptions are cases where emission maps to the magnetic axis [14-16]. In contrast, the frequency of ICE measured on NSTX and NSTX-U is approximately half way between the edge and the core ion-cyclotron frequency. This is seen in Fig. 1 for a 3.4 kG NSTX shot, and in Fig. 2 for a 5.9 kG NSTX -U shot. There is a narrow band of magnetic fluctuations, identified in Fig. 1a as ICE (Ion Cyclotron Emission), whose frequency varies from ≈2.3 MHz at 0.175 s, up to ≈2.5 MHz at 0.195 s and then back down. The yellow-colored band spans the range of the fundamental deuterium ion-cyclotron frequency from the outboard plasma edge to the magnetic axis. The ICE frequency within each shot increases as the plasma is moved inward in major radius to higher field, demonstrating the cyclotron frequency scaling of the ICE. The ICE frequency mapping to an ion-cyclotron resonance deeper in the plasma presents a challenge to theory which predicts, among other things, that the ICE should be strongly damped by the cyclotron resonance with the thermal ions.

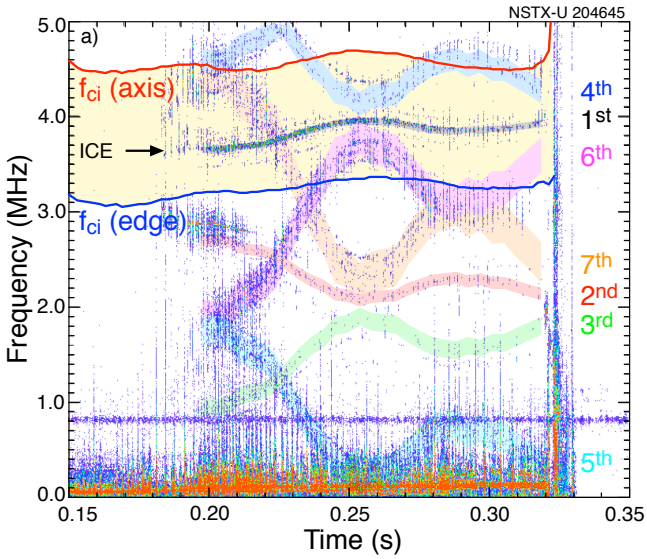

Fig. 2. a) Spectrogram of magnetic fluctuation acquired at a digitization rate of 10 MHz. The Deuterium ion cyclotron frequency at the plasma edge and on axis indicated in blue/red, the colored bands ($\delta f/f \approx 1\%$) show aliased harmonics of the fundamental f_{ci} for deuterium, as indicated, ($I_P \approx 0.6$ MA, $P_{NBI} \approx 5.8$ MW, $B_{tor} \approx 5.9$ kG)

As with observations of ICE on higher field tokamaks, higher harmonics (up to the seventh) have been seen on NSTX/NSTX-U. This is in contrast to the CAE studied on NSTX where higher harmonics, while theoretically possible, are not seen. The diagnostic systems on NSTX and NSTX-U were not designed to study instabilities with frequencies above the ion cyclotron frequency, and the higher ICE harmonics are typically aliased, complicating interpretation of the spectra. The aliased higher harmonics are seen in Figs. 1 and 2 and are identified by mapping the expected harmonic frequencies, based on the fundamental harmonic frequency, onto the spectrogram as the labeled colored bands.

The dominant energetic particle species in these plasmas are the deuterium neutral beam ions. However, the D-D fusion reactions produce three other fast-ion species in roughly equal numbers, 1.01 MeV Tritons, 3.02 MeV protons, and 0.82 MeV He^3. We can estimate an upper limit for the fusion products populations by assuming no losses and neglecting slowing down. Then the total number of fusion product ions can be estimated from the integral in time of the total neutron rate, S. This yields $N_{fp} = \int S/2\ dt \approx 1 \times 10^{12}$ at 0.22s for the case of the shot shown in Fig. 2. TRANSP calculates the volume integral of beam ions to be $N_{bm} \approx 4.5 \times 10^{17}$ at 0.22s, so the maximum average relative density of each of the fusion products is $N_{fp}/N_{bm} \approx 2.2 \times 10^{-6}$, much smaller than the average beam-ion density. Further, the very energetic fusion products are susceptible of large losses as a result of the large radial excursions of their orbits. For example, in the 2.6 kG plasmas, the Larmor radius of the tritons and protons is ≈ 60cm, and for the He^3, the Larmor radius is ≈ 30cm, thus a large fraction of the fusion products are likely to be lost. In Fig. 3 are shown the profiles of the ion cyclotron frequencies for the D-D fusion products (Tritium, Deuterium, Helium-3 and Hydrogen) *vs.* major radius and the measured ICE frequency (vertical dashed line) for the plasma shown in Fig. 2 (at 0.298s). The ICE frequency is significantly lower than the edge cyclotron frequencies for the proton (H) and the He^3. The tritium cyclotron frequency is well below the measured ICE frequency. The ICE is thus reasonably assumed to be driven by the non-thermal deuterium beam ions.

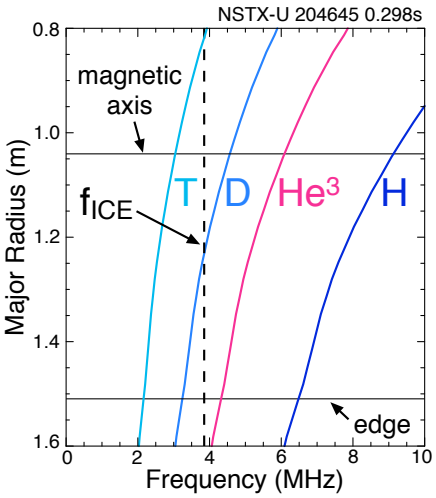

Fig. 3. Cyclotron frequency profiles for the principal energetic ion species, compared to the ICE frequency.

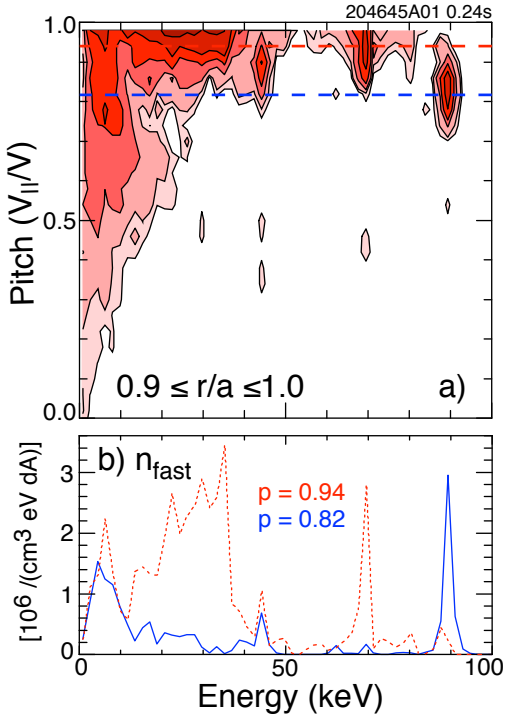

Fig. 4. Beam ion distribution function in outboard plasma edge (±60°) showing bump-on-tails at the beam injection energies of 80 kV and 90 kV.

The fusion alphas born on barely confined orbits were assumed to provide the drive for ICE on JET. The barely confined alphas would create a co-propagating bump-on-tail at the plasma edge in the fusion-α distribution. The beam-ions in NSTX-U can produce a similar edge fast ion distribution. Beam ions deposited on the high field side of the magnetic axis can be born on orbits that take them through the plasma edge on the outboard mid-plane. This is only true for the three sources with tangency radii inboard of the magnetic axis. In Fig. 4a is shown the fast ion distribution on the outboard plasma edge as calculated with the NUBEAM code in TRANSP for the shot in Fig. 2. In this shot there

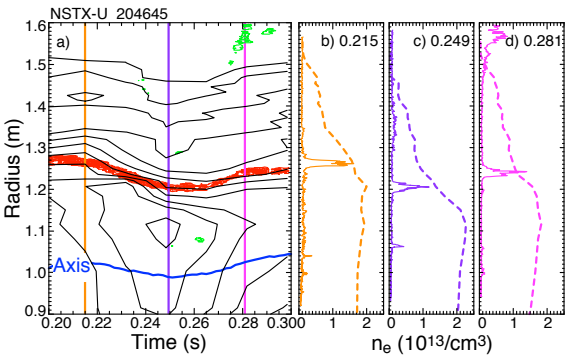

Fig. 5. a) Contours of electron density (black) with a magnetic spectrogram overlaid (red - fundamental, green - higher harmonics), where the spectrogram frequency has been mapped to the radial profile of the ion-cyclotron frequency. The blue curve shows the location of the magnetic axis, b-d) density profile and fluctuation spectra (a.u.) mapped to radius at indicated times.

are two clear bump-on-tails from the beam sources 1c and 1b with tangency radii of 60 cm and 70 cm, respectively (Fig. 4b). The source voltages were 90 kV and 69 kV. There was an additional source, 2b, with tangency radius of 120 cm (outside the magnetic axis) at 80 kV, and a very weak bump-on-tail can be seen from that. The width in energy of the peaks at 69 kV and 90 kV is about $\delta E/E \approx 0.05$, which might be sufficiently narrow to satisfy the requirement for destabilizing the MCI [24,26].

In Fig. 5a are shown contours of the density profile (black) for the shot shown in Fig. 2. The ICE frequency spectrum (red contours) is time-dependently mapped to the radial profile of the ion cyclotron frequency and overlaid on the density contours. The blue curve in Fig. 5a indicates the location of the magnetic axis. The evolution of the ICE frequency is correlated with movement of the plasma, that is, as the plasma is shifted inwards towards higher magnetic field the ICE frequency increases. The radial location of the mapped ICE frequency peak roughly follows the contours of density, or perhaps more accurately, follows the location of an apparent internal transport barrier. This is seen more clearly in the time slices of magnetic fluctuation spectrum and density profile at 0.215s, 0.249s and 0.281s in Figs. 5b-d, respectively. The ICE maps to a region of strong local density gradient in ≈80% of the approximately 100 shots from NSTX-U examined so far. In the others, the ICE maps just inside, or just outside, the strong density gradient region, or there wasn't a strong local density internal transport barrier. This location is also typically a local minima in the radial profile of the Alfvén velocity. Similar observations were made for the earlier NSTX shots.

The internal density transport barrier also approximately coincides with momentum and ion temperature transport barriers. We show in Fig. 6 data from a shot similar to that shown in Fig. 5. This shot also had the inward, then outward motion of the strong density gradient region as seen in Fig. 6a. Profiles of the toroidal velocity (shown as rotation frequency in Fig. 6b, orange curve) and ion temperature (Fig. 6b, blue curve) were available around

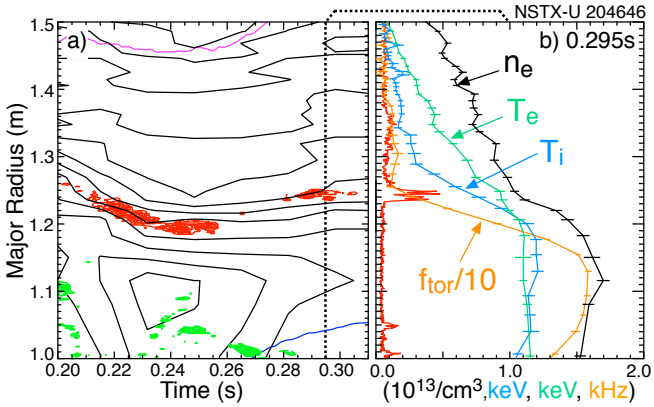

Fig. 6. a) ICE spectrogram mapped to major radius (red) overlaid on density contours (black), b) magnetic fluctuation spectrum mapped to major radius (red), electron density (black) and ion temperature (blue) profiles at 0.298s.

0.3s. The electron density profile (black), electron temperature (green) and the mapped spectrum of magnetic fluctuations (red) are also shown. In this and other examples, both the toroidal velocity and the ion temperature are very low outside the mapped radius of the ICE. This is even true in H-mode cases where the radial change in density can be quite small at the mapped ICE location, but the ion temperature still remains very low outside the ICE radius, while the ICE is present. The lower ion temperature may reduce thermal ion damping of the ICE.

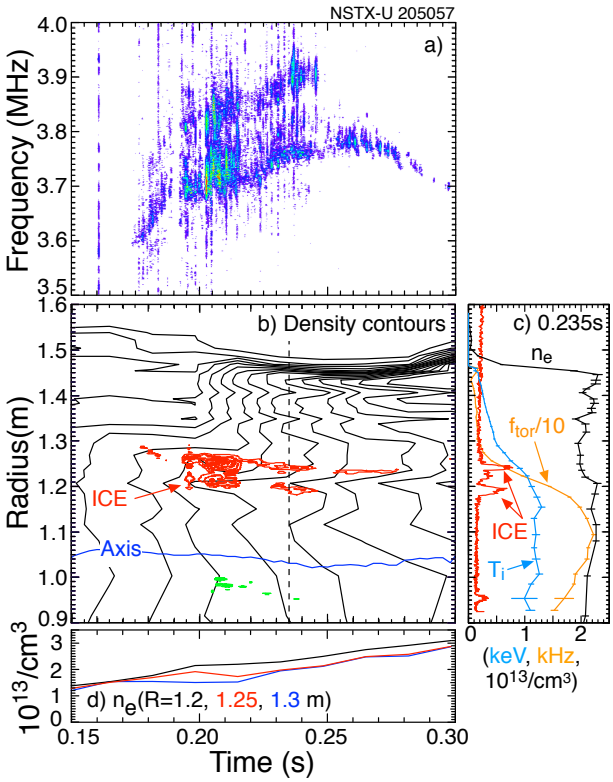

Fig. 7. a) magnetic fluctuation spectrum showing ICE, b) Contours of electron density (black) with magnetic spectrogram overlaid (red), where spectrogram frequency has been mapped to major radius of ion-cyclotron frequency, c) density profile (black), fluctuation spectra (red) and ion temperature (blue) at 0.232s, d) density evolution at three major radii, black at R=1.2m, red at R=1.25m and blue at 1.3m.

In Fig. 7 is shown an example of ICE during an H-mode transition in NSTX-U. In Fig. 7a the spectrogram shows the ICE frequency slowly increasing in time, consistent with a small inward motion of the plasma. In Fig. 7b the ICE frequencies are mapped to the time-dependent radial profile of the ion cyclotron frequency and overlaid on contours of density. This plasma density was increasing prior to the H-mode transition, and the density continued to increase afterwards. The mapped ICE location remains correlated with a weak internal density transport barrier and with the ion temperature transport barrier as seen in Fig. 7c. This example is primarily of interest in that the density increases substantially during the period of ICE emission. The density increase is clear in Fig. 7d where the density roughly doubles between 0.15 s and 0.3 s at the major radius of the mapped ICE location. The wave frequency increases slightly as the density increases, rather than dropping by the roughly 40% that would be expected for an Alfvénic mode. The 40% drop in frequency is supported by simulations with the CAE code [40]. This independence of the ICE frequency from plasma density was also observed in experiments on LHD [13] and TUMAN-3M [15]. In contrast, CAE on NSTX show a clear Alfvénic scaling of frequency with density.

IIb. ICE fine-structure, bursting and time coherence.

Figure 8 shows an example of ICE where the fundamental ICE emission peak exhibits a complicated fine structure reminiscent of that reported on JET [8]. The emission comes in short, irregular bursts in roughly six frequency bands with an average spacing between bands

of the order of 110 kHz, or $\delta\omega/\omega \approx 2.7\%$. While the multiple frequency peaks seen near the fundamental harmonic are reminiscent of the frequency splitting reported on JET, on JET the frequency splitting was not seen on the fundamental and second harmonic, although that may have been due to lack of resolution in the frequency spectra. On NSTX, the frequency splitting fine structure has been seen on all harmonics. On conventional tokamaks the splitting of ICE peaks was predicted to scale like $\delta\omega/\omega \approx \varrho_L/R\ V_{beam}/V_{Alfvén}\ (1+p_r^2)$ for ICE [29,30], where p_r is the pitch of resonant fast ions, arising from drift corrections to the beam velocity. The above equation predicts a splitting of $\delta\omega/\omega \approx 0.15$ - 0.17, using $\varrho_L/R \approx 0.08$, $V_{beam}/V_{Alfvén} \approx 1.24$ - 1.45 and $p_r \approx 0.7$, approximately six times that seen in the experiment.

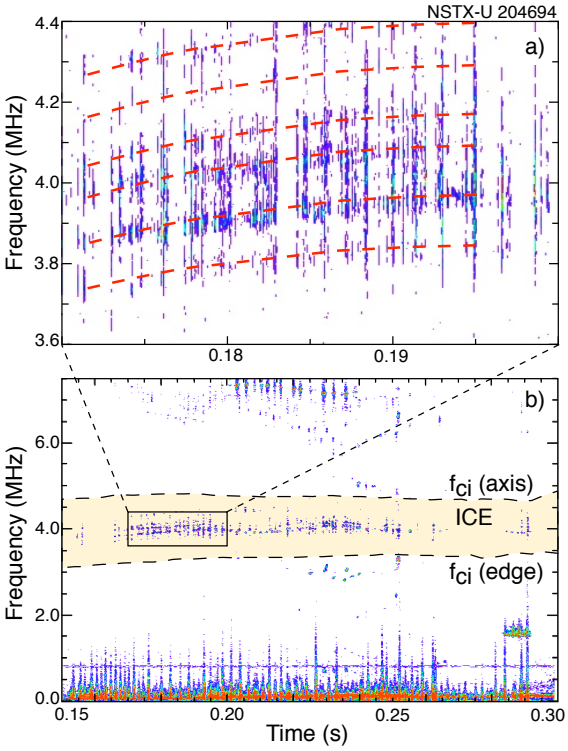

Fig. 8. b) Detail of spectrogram illustrating multiple frequency bands in fundamental ICE, b) spectrogram of magnetic fluctuations with the fundamental ICE harmonic in the high-lighted area. ($I_P \approx 0.6$ MA, $P_{NBI} \approx 5.5$ MW, $B_{tor} \approx 5.9$ kG)

The ICE is not continuous, but has a bursty character, with varying burst lengths and amplitudes. Bursting was also seen in some of the early studies of ICE on higher field tokamaks [13,16], although many early measurements lacked the time resolution to resolve short bursts. In Fig. 9a is shown a spectrogram of magnetic fluctuations covering the frequency range of the fundamental deuterium ICE showing multiple, short period bursts (data again from the example shown in Fig. 2). In Fig. 9b is shown the root-mean-square (rms) magnetic fluctuation level over the frequency range from 3.8 MHz up to 4.0 MHz. The period and amplitude of the bursts are irregular, but in this time interval roughly two to three bursts per millisecond is typical.

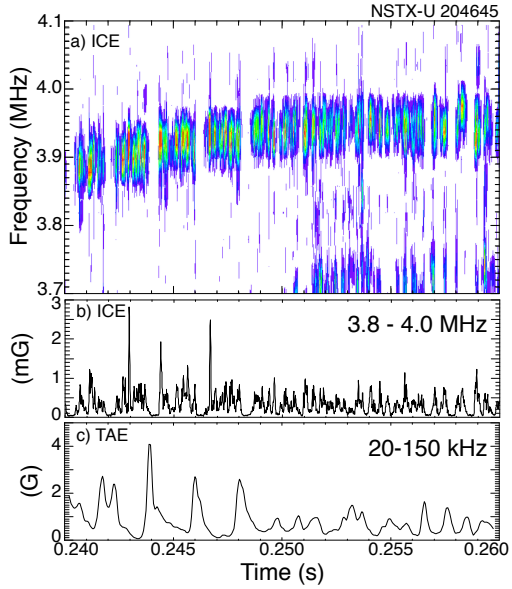

Fig. 9. a) spectrogram of magnetic fluctuations showing bursts of Ion Cyclotron emission, b) rms amplitude of the ICE bursts, c) rms amplitude of lower frequency Toroidal Alfvén eigenmodes.

There are four short, nearly quiescent periods between 0.24 s and 0.25 s in Fig. 9b. These are correlated with strong bursts of Toroidal Alfvén Eigenmode (TAE) activity visible in the rms fluctuation level in the TAE frequency range as shown in Fig. 9c. The strong ICE bursts follow a

short quiescent period after each TAE avalanche burst. The TAE avalanches are known to perturb the fast ion population by reducing the energy of the fast ions and by shifting them radially outward. Generally, ICE is believed to be excited by energetic ions near the plasma edge, so it is surprising that the avalanches, which move fast ions towards the plasma edge, suppressed the ICE for a short period. However it could be consistent with an assumption that the ICE, and the fast ions that excite it, come from deeper in the plasma, near the location of peak TAE amplitude.

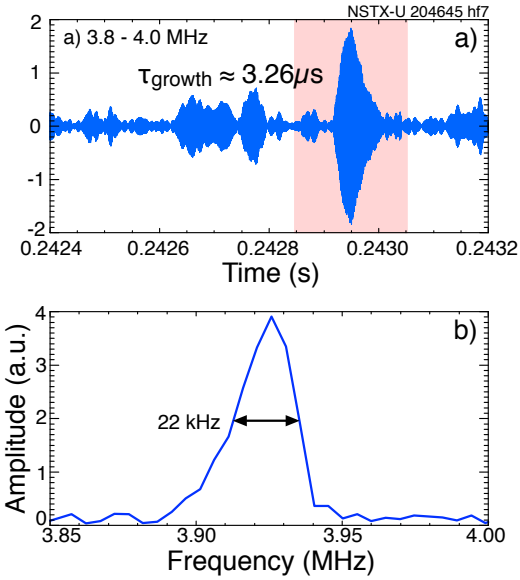

Fig. 10. a) Digitally filtered ICE fluctuations for example shown in Fig. 5, Fourier transform of pink region in a) showing FWHM of ≈22 kHz.

A digitally filtered Mirnov coil signal of the largest of the ICE bursts in Fig. 9b at ≈ 0.243 s is shown in Fig. 10a. The duration of the large burst is about 100 μs. The Fourier transform of the pink region in Fig. 10a is shown in Fig. 10b, where the full-width at half-maximum of the spectral peak is about 20 kHz ($\delta\omega/\omega \approx 0.5\%$), a width consistent with the duration (or growth/damping rate) of the burst, indicating that this is a very temporally coherent signal. The peak width, normalized by the local gradient of the cyclotron frequency (≈30 kHz/cm) gives a "resonance layer" width of ≈0.7 cm, that is where the ion cyclotron frequency would match the mode frequency. The initial growth rate of this burst is $\gamma \approx 3.07 \times 10^5$/s or $\gamma/\omega \approx 1.25\%$.

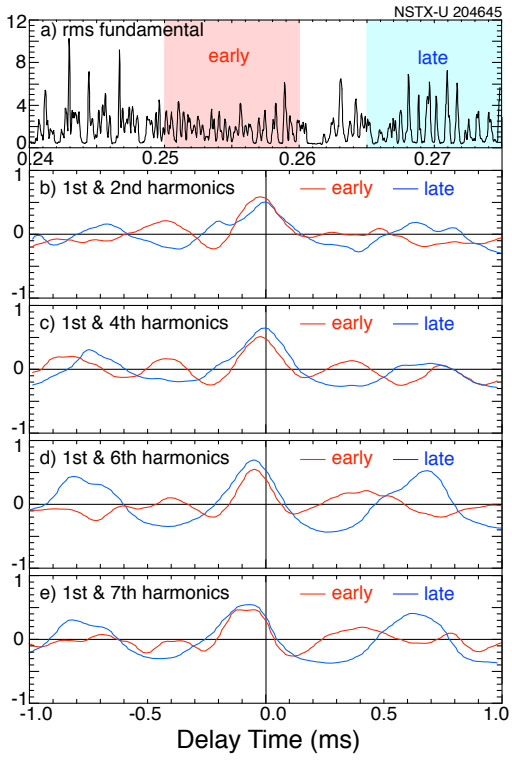

Fig. 11. Cross-correlation of fundamental ICE rms fluctuations with 2nd, 4th, 6th and 7th ICE harmonics. Red curves are correlations done if first time window indicated in 8a by pink band, blue curves are correlations done in second time window indicated by blue band.

Theoretical work for conventional aspect ratio tokamaks has suggested that the lower frequency harmonics are linearly stable or have lower growth rates than higher harmonics, and are non-linearly excited by the higher harmonics [18,19]. This prediction is consistent with some of the experimental data on conventional aspect ratio tokamaks. On NSTX-U the bursts at each of the harmonics are weakly correlated in time, indicating that there is indeed some coupling between harmonics, although it is not clear whether that is wave-wave coupling or a coupling through the fast ion population. The time-delay correlation of the rms-fluctuation levels, that is a correlation of the

burst times, between harmonics for the data shown in Fig. 2 are shown in Fig. 11. Time-delay correlations of the rms amplitude of the fundamental harmonic with the 2nd, 4th, 6th, and 7th harmonics are shown in Figs. 11b through 11e. The third harmonic was too weak and the fifth harmonic was aliased into the lower frequency band dominated by toroidal Alfvén eigenmode activity, so could not be included. The figure covers the time range from 0.24s to 0.275 seconds when these (aliased) harmonics were well separated in frequency. Time-delay correlations were calculated over the two time windows indicated by the pink and blue bands in Fig. 11a. The harmonic bursts are correlated at the $\approx 50\%$ level in each window (Figs. 11b through 11e), but the bursts in the second window (blue) are nearly periodic, which shows up in the time-delay correlations as a roughly sinusoidal oscillation.

An interesting observation is that the bursts of higher harmonics slightly lead the bursts of the fundamental harmonic. The delay appears to increase roughly linearly with harmonic number and is seen best in Fig. 11e where the 7th harmonic bursts leads the fundamental bursts by $\approx 90\ \mu$s. The apparent lag of the fundamental bursts is much larger than an estimate of the group delay through the sensor system (0.1 to 0.2 μs) and could indicate that bursts of higher harmonics trigger the lower harmonic bursts.

In a few low field examples, the ICE was not bursting, but showed as a continuous mode for bursts lasting as long as 3 - 4 ms. (The bursts occurred between EPMs.) This burst duration was sufficiently long so as to encompass several bursts of the lower frequency Global Alfvén eigenmodes. This led to the interesting observation of a non-linear three-wave coupling between the GAE and the ICE. In Figure 12 is shown a spectrogram of magnetic fluctuations in the frequency range up to 3 MHz. The fundamental and fourth harmonic (aliased) ICE are indicated with the numerals "1" and "4" in black and blue, respectively. Sidebands from coupling of the GAE to the fundamental ICE are clearly visible, with the ICE-GAE sidebands highlighted by the pink-shaded regions. Fig. 12b expands a small region of the spectrogram (as indicated) showing a portion of the upper sideband of the first harmonic ICE. Fig. 12c shows the rms amplitude of the fundamental ICE. Fig. 12d similarly shows an expanded view of GAE activity in the same time interval, matching the spectrogram in Fig. 12b. Similar coupling, although not as uniquely identifiable, is seen between the ICE and the lower frequency

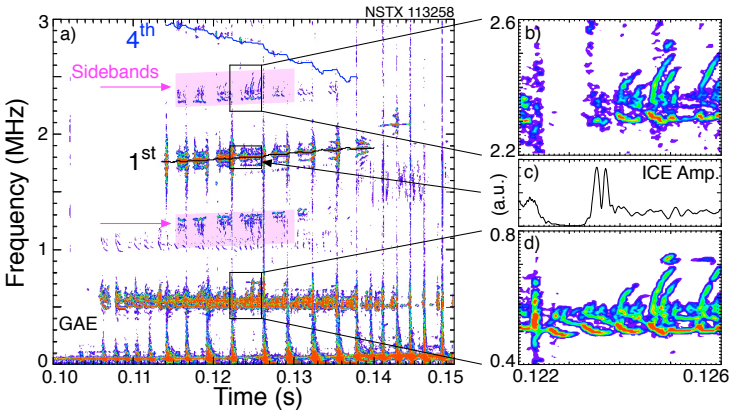

Fig. 12. a) Spectrogram showing ICE from a 2.6 kG plasma with 3.5 MW of neutral beam heating, b) expanded region showing upper sideband of ICE-GAE coupling, c) rms amplitude of fundamental ICE, d) expanded region showing GAE.

fishbone activity. The non-linear coupling of the GAE with ICE provides strong evidence that the ICE is an eigenmode of the plasma.

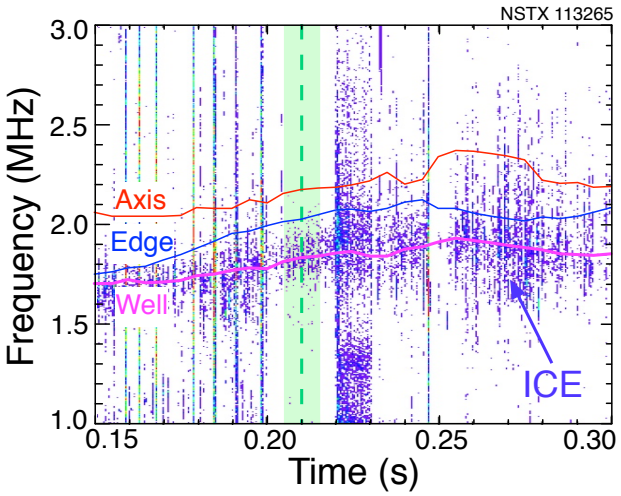

Fig. 13. a) Spectrogram showing ICE from a 1 MA, 2.6 kG plasma with 2.7 MW of neutral beam heating. Magenta curve is the ion-cyclotron frequency at the local minimum in mod(B), red and blue curves are the ion-cyclotron frequencies at the axis and plasma outboard edge, respectively.

In the presence of a 'magnetic well', the ICE frequency peak broadens with a peak width of $\delta\omega/\omega \approx 10\%$ to 15%. This is illustrated in Figs. 13 and 14 which show the spectrum of ICE magnetic fluctuations in the broad frequency range between ≈1.5 MHz and ≈2.0 MHz. In Fig. 13 the magenta curve shows the evolution of the deuterium ion cyclotron frequency at the magnetic well minimum, which roughly follows the peak of the ICE spectrum. The red and blue curves show the ion-cyclotron frequency evolution at the magnetic axis and at the outboard midplane plasma edge, respectively which are both higher than the ICE frequency peak. Magnetic wells are formed during high-current, high-β, low field operation of NSTX; the relatively strong poloidal field at the plasma edge, together with the radial decay of the toroidal field on the outboard side, can create a local minimum in the mod(B) profile. As in previous examples, the frequency of the ICE can be related to ion cyclotron frequency on the outboard side of the plasma at approximately the half-radius.

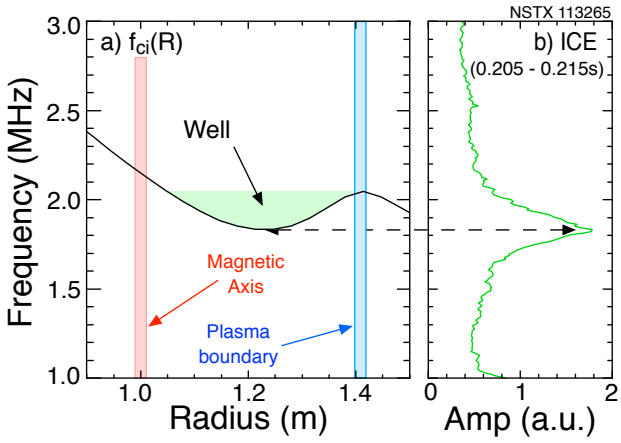

Fig. 14. a) Profile of ion-cyclotron frequency showing local minimum near R = 1.2m, radii of magnetic axis, boundary are indicated, b) spectrum averaged from 0.205 to 0.215s.

Fig. 14a shows the radial profile of the local ion-cyclotron frequency *vs.* major radius (black curve), with a minimum near R = 1.2m. The spectrum shown in Fig. 14b is time-averaged between 0.205s and 0.215s (the green band in Fig. 13). For previous examples, the narrow frequency peak, together with the local gradient in magnetic field strength implied a strong spatial localization, $\delta R \approx$ 1cm, for the resonant drive of the ICE. This, despite the rather large larmor radius for beam ions in NSTX which can reach ≈15cm. Under the conditions of a magnetic well, the broadening of the ICE frequency peak and the longer magnetic field gradient scale length suggest the ICE resonant layer could encompass a large fraction of the minor radius. Ther velocity profile data for this shot shows a strong gradient just inside the well minium, but no

evidence of a strong transport barrier as in other shots. This may represent a different type of ion-cyclotron emission.

IIc. Spatial structure

Measurements of the poloidal and toroidal structure of ICE have been made on the conventional aspect ratio tokamak JT-60U [11]. Toroidal propagation was found for ICE from fusion products, but not for the ICE associated with the deuterium beam ions. The ICE described here is measured with a toroidal and poloidal array of magnetic sensors, offering the possibility of wavelength and mode polarization measurements. However, the signal-to-noise levels for the ICE are low and the frequencies are at or above the nominal design bandwidth of the system so measurements of phase-shifts between detectors are less precise than for lower frequency, higher amplitude oscillations. The ICE also typically appears in short pulses, making discrimination against the noise background more difficult. Exceptions were found in very low field ($B_{tor} \approx 2.6$ kG) NSTX plasmas where roughly constant ICE signals were seen lasting up to 4 ms. In some of those cases the ICE frequency was 1.8 to 1.9 MHz which made analysis with the twelve coil array acquired at a 4 MHz digitization rate possible. The greater number of coils spanning a larger toroidal range improves the mode identification (although the results were consistent with analysis using the three-coil higher bandwidth data for that shot). The result is shown in Fig. 15 for the same shot used to illustrate 3-wave coupling of GAE with ICE in Fig. 12. The ICE is seen as the black contours between -1.8 MHz and -1.9 MHz in Fig. 15 and is counter propagating with a toroidal mode number of n = -1. The counter-propagating ICE should have a frequency that is down-shifted from the cyclotron frequency, but the ICE frequency is already higher than the edge cyclotron frequency. The GAE are also counter propagating but with shorter wavelengths, *i.e.*, higher toroidal mode numbers of predominantly n = -5.

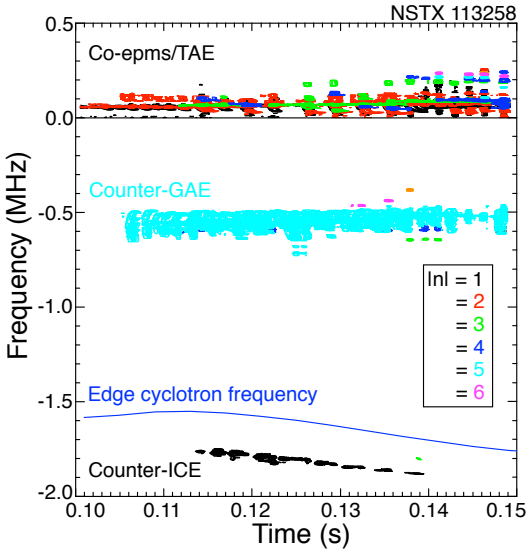

Fig. 15. Spectrogram with contours colored to indicate toroidal mode number. Black contours at bottom are the n=-1, counter propagating ICE and cyan contours between -0.5 and -0.7 MHz are n=-5 counter propagating GAE.

In NSTX-U the ICE frequency was near 4 MHz and mode fitting was only possible using the new toroidal array of eight coils. Due to the sparser array, the fits were often somewhat ambiguous, but the best fits are consistent with a counter-propagating mode with toroidal mode number of n = -1. The array consists of three groups of sensors with each group separated by roughly 90° toroidally. The distribution of the sensors into three clumps roughly 90° apart makes discrimination between n = -1 and n = +3 difficult. The array used on NSTX-U also includes coils oriented to measure the toroidal magnetic fluctuations. With these

measurements it was possible to determine that the magnetic fluctuations are nearly aligned with the edge equilibrium magnetic field, illustrating the compressional nature, as expected, for the ICE.

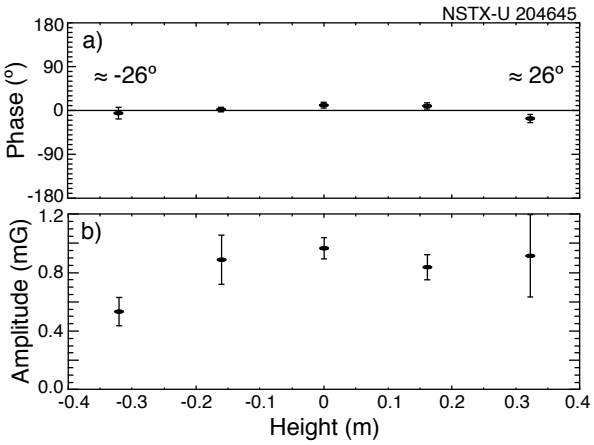

Fig. 16. a) Phase and b) amplitude data from the poloidal Mirnov coil array for the strong ICE burst shown in Fig. 4.

NSTX-U also has a poloidal array of five Mirnov coils covering a poloidal range of 0.7 m, or approximately 50º, centered on the outboard midplane. The phase and amplitude data vs. vertical displacement from the midplane (in meters) are shown in Figs. 16a and 16b, respectively. For this example there is no significant phase variation over the poloidal range of the array, indicating that there is no wave propagation in the poloidal direction. However, in other cases poloidal propagation was seen. Determination of a poloidal mode number from a partial array such as this on the outboard side is not possible without a model for the poloidal variation of the poloidal wavelength.

The low toroidal mode numbers suggest that a Doppler-shifted cyclotron resonance might be responsible for exciting the ICE instability at a frequency above the edge ion cyclotron frequency by the edge bump-on-tail shown in Fig. 4. The resonance condition for fast ions with a co-propagating mode, including the next order fast ion drifts, is $\omega_{ICE} = \omega_{ci} + |k_{||} \pm s/qR|/V_{b||}$. The $k_{||}$ needed to satisfy this resonance condition can be estimated from the observed mode frequency, the edge ion cyclotron frequency and the parallel velocity of the fast ions. For the example shown in Figs. 2 and 4 the edge ion cyclotron frequency is ≈ 3.3 MHz, the mode frequency is ≈ 3.93 MHz and the parallel velocity of fast ions in both of the bump-on-tails is ≈ 2.4×10^8 *cm/s* (the higher pitch compensates for the lower voltage). With these numbers, the resonance equation can be solved to find $|k_{||} R \pm s/q| \approx 2.2$. This would be roughly consistent with a co-propagating mode with toroidal mode number $n = 3$, found as one of the potential mode numbers for the ICE in this shot. However, the analysis shown in Fig. 14 clearly excluded a co-propagating $n = 3$ mode.

IIe. Correlation of ICE with plasma parameters

A database of parameters during times of ion cyclotron emission was constructed for the NSTX-U shots in the range 204500 - 205088. This comprises the range where noise compensation was available to reduce the broad-band pick-up from the unshielded switching power amplifiers used for error field correction. Time intervals where ICE was present were determined for each shot, and within those time intervals plasma parameters, including parameters for each of the neutral beam sources and plasma density, were collected at the Thomson scattering times (typically the Thomson system collects electron temperature and

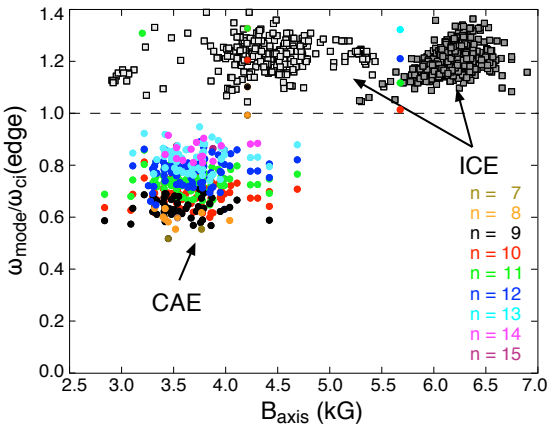

Fig. 17. Frequency of co-propagating CAE, normalized to ω_{Dci} at plasma edge vs. magnetic field on axis. CAE toroidal mode numbers from n = 7 to n = 14 as indicated. Square points show similarly normalized ICE for NSTX (light grey) and NSTX-U (dark grey).

density profiles at a rate of 60 Hz). Spectra of magnetic fluctuations were calculated around the Thomson times and averaged over an approximately 16.7 ms window (the spacing of the Thomson scattering times). The rms fluctuation amplitude was collected in six frequency bands, with the sixth band covering the fundamental ICE frequency range from 3.5 MHz up to 4.5 MHz.

In Fig. 17 are shown the ICE frequencies normalized to the edge deuterium cyclotron frequency for early NSTX shots when a 10 MHz digitizer was available and for the NSTX-U shots. The data are graphed *vs*. the magnetic field on axis as determined from equilibrium reconstructions, thus including paramagnetic and diamagnetic corrections as well as variations from shifts in the plasma major radius. The ICE frequencies scale roughly linearly with the toroidal field, thus maintaining a roughly constant ratio to the edge cyclotron frequency. Also shown are the frequencies from a representative sample of co-propagating CAE on NSTX, normalized to the edge deuterium cyclotron frequency. (Counter-propagating CAE have lower frequencies, typically less than 0.4 f_{ci}.) The frequency of the co-propagating, high-n CAE in NSTX H-mode plasmas seldom exceeds the edge deuterium cyclotron frequency, however in low density exceptions, at all toroidal fields, the co-propagating CAE can have frequencies higher than the edge deuterium cyclotron frequency. Similar observations were reported for co-propagating CAE in low field MAST plasmas [39]. The frequencies of the single example, so far, of CAEs in an NSTX-U shot were all above the edge ion cyclotron frequency. As for the ICE, the normalized co-propagating-CAE frequencies appear relatively constant as the toroidal field is increased.

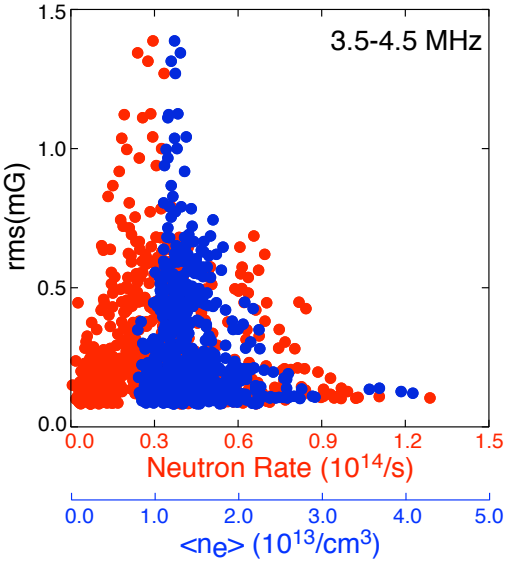

Fig. 18. Correlation of ICE instensity (fluctuation amplitude between 3.5 MHz and 4.5 MHz) with neutron rate (red points, red axis) and density (blue points, blue axis).

Experiments on JET found a linear correlation of the fusion products ICE amplitude with the neutron rate [17]. The correlation of ICE intensity with neutron rate was also not so strong in TFTR, and one hypothesis for the difference was that in the JET H-mode plasmas, the fusion α's remained super-Alfvénic out to the plasma edge (but presumably not past the density

pedestal). In contrast, in the higher field, peaked density TFTR supershots the fusion α's would be sub-Alfvénic at the plasma edge [9,28]. In Fig. 18 the correlation of ICE intensity with neutron rate is also weak in NSTX-U. ICE on NSTX and NSTX-U was most typically seen early in the discharge, often during the current ramp, in relatively low density plasmas. The NSTX shots were typically in H-mode plasmas with $V_{beam} > V_{Alfvén}$, even at the plasma edge. In contrast, many NSTX-U shots remained in L-mode with peaked density profiles, and in some cases $V_{beam} \approx V_{Alfvén}$ at the plasma edge, but typically $V_{beam}/V_{Alfvén} > 1$ at the mapped ICE location.

III. Discussion and summary

A highly coherent instability in the deuterium cyclotron frequency range is seen on NSTX and NSTX-U. We have described observations of magnetic fluctuations in the ion-cyclotron frequency range on NSTX and NSTX-U. The ICE on NSTX/NSTX-U appear similar to the ion cyclotron emission (ICE) seen in conventional tokamaks. The emission frequency matches the cyclotron frequency of the neutral beam ions and multiple harmonics (up to the seventh) have been observed. As on conventional tokamaks, the emission frequency doesn't follow an Alfvénic scaling with density, as seen for compressional Alfvén eigenmodes, but does show a linear scaling with local magnetic field strength. Similar to previous measurements on conventional tokamaks, the emission is spatially coherent with a relatively long wavelength. As on conventional tokamaks, the frequency peaks at each harmonic can be split into two or more peaks. The ICE on NSTX/NSTX-U consists of short bursts typically 10's of μs in duration, leading to the interesting observation that bursts at each of the harmonics are correlated, and that the higher harmonic bursts lead the bursts at lower harmonics. However, it is also seen that higher harmonics are often sufficiently weak to be below the detection threshold. The bursting of ICE emission was also reported on conventional tokamaks. No correlation between neutron rate and ICE amplitude is seen, consistent with some previous studies. In these respects, the ICE seen on NSTX/NSTX-U bears a strong resemblance to previous reports of ICE on conventional, higher field, tokamaks.

There are also significant differences between previous observations of ICE and the ICE on NSTX/NSTX-U. The frequency of ICE in conventional tokamaks is typically near the ion cyclotron frequency of the energetic fast ions at the plasma edge (with some exceptions). In NSTX and NSTX-U the ICE frequency corresponds to the beam-ion cyclotron frequency deeper in the plasma, near the location of an internal ion energy and density transport barrier. This correlation appears to be quite strong, and suggests that the presence of the transport barrier plays an important role in the instability.

The low field, hence low frequency of the ICE on NSTX and NSTX-U allowed for new measurements of ICE characteristics. In a few very low field cases there was a clear identification of the ICE as an n = -1, counter-propagating wave. This identification of the

toroidal wavelength was consistent with ICE seen at higher fields, although the measurements made in high field plasmas were less conclusive. The measured emission shows a compressional polarization consistent with the expectation that ICE is a compressional Alfvén wave or eigenmode.

A possibly different type of ICE was seen in low field, high beta plasmas with a magnetic well. The ICE frequency becomes much less coherent in the presence of an outboard magnetic well, and the frequency of the ICE is significantly *lower* than the edge deuterium ion-cyclotron frequency. The magnetic well was created in a very low field, high current plasmas with plasma beta of >20%. The peak of the ion cyclotron emission corresponds roughly to the deuterium ion cyclotron frequency at the well minimum. The width of the emission peak is $\delta\omega/\omega \approx 13\%$, which is much broader than the typical ICE frequency peak. The broad, quasi-coherent frequency peak, and the emission frequency less than the edge frequency suggest that this type of ICE is different than the other examples shown here.

High beta, low field spherical tokamaks have opened a new regime for studies of ion cyclotron emission (ICE) from plasmas. While overall the observations of ICE on NSTX/ NSTX-U bear a strong resemblance to previous studies of ICE on conventional tokamaks, the observations reported here may help guide the development of a more comprehensive model of ICE. A better understanding of ICE is necessary if ICE is to be used as a fast ion diagnostic on ITER. The data presented here is not the result of dedicated experiments, but just accumulated during a broad range of experiments to study other issues. In the future, we hope that dedicated experiments and diagnostic improvements will provide further clarification of ICE characteristics.

Acknowledgements

The authors appreciate the support of the NSTX project in the construction and installation of the high-frequency magnetic sensor arrays that made these observations possible. This work was supported by US DOE Contract DE-AC02-09CH11466

Bibliography:

Historical observations of ICE:

[1] *Microinstability Limitations of the DCX-1 Energetic Plasma*, J. L. Dunlap, G. R. Haste, C. E. Nielsen, H. Postma, and L. H. Reber, Phys. Fluids **9** (1966) 199.

[2] *Radiation and Ion Energy Distributions of the DCX-1 Plasma*, J. L. Dunlap, C.F. Barnett, R.A. Dandi, H. Postma, Nucl. Fusion Supplement, Part 1, p233 (1962).

[3] *Excitation of Ion Cyclotron Harmonic Waves in a Plasma by a Perpendicularly Injected Electron Beam*, T. Yamamoto, T. Suito, Journal of the Physical Society of Japan **24** (1968) 953.

[4] *High Frequency Emission from TFTR plasmas,* G.J. Greene, P.L. Colestock, E.D. Fredrickson, J.C. Hosea, K.M. McGuire, J.R. Wilson, K.M. Young, in Controlled

Fusion and Plasma Heating (Proc. 15th Eur. Conf. Dubrovnik, 1988), Vol. 12B, Part I, European Physical Society, Geneva (1988) 107.

[5] *Superthermal Radiation from Fusion Products in JET,* Cottrell, G.A., Dendy, R.O., Phys. Rev. Lett. **60** (1988) 33.

[6] *Sawtooth oscillations in ion cyclotron emission from JET*, P. Schild, G. A. Cottrell, R. O. Dendy, Nucl. Fusion **29** (1989) 834.

[7] *Measurement of Ion Cyclotron Emission and ICRF-driven waves in TFTR,* G. J. Greene and the TFTR Team, in *Proceedings of the 17th European Conference on Controlled Fusion and Plasma Heating*, Amsterdam, Netherlands, 1990, edited by G. Briffod, A. Nijsen-Vis, and F. C. Schüller (European Physical Society, Petit-Lancy, Switzerland, 1990), Part IV, Vol. 14B, p. 1540.

[8] *Ion Cyclotron Emission Measurements During JET Deuterium-Tritium Experiments,* G. A. Cottrell, V. P. Bhatnagar, O. Da Costa, R. O. Dendy, J. Jacquinot, K.G. McClements, D.C. McCune, M.F.F. Nave, P. Smeulders, D.F.H. Start, Nucl. Fusion **33** (1993) 1365.

[9] *Ion cyclotron emission on the Tokamak Fusion Test Reactor*, Cauffman, S., Majeski, R., Rev. Sci. Instrum. **66** (1995) 817.

[10] *Alfvénic Behaviour of Alpha Particle Driven Ion Cyclotron Emission in TFTR*, Cauffman, S., Majeski, K.G. McClements, R.O. Dendy, Nucl. Fusion **35** (1995) 1597.

[11] *Observation of spontaneously excited waves in the ion cyclotron frequency range on JT-60U*, M. Ichimura, H. Higaki, S. Kakimoto, Y. Yamaguchi, K. Nemoto, M. Katano, M. Ishikawa, S. Moriyama and T. Suzuki, Nucl. Fusion **48** (2008) 035012.

[12] *Observation of Ion Cyclotron Emission Owing to DD Fusion Product H Ions in JT-60U*, Shoichi Sato, Makoto Ichimura, Yuusuke Yamaguchi, Makoto Katano, Yasutaka Imai, Tatsuya Murakami, Yuichiro Miyake, Takuro Yokoyama, Shinichi Moriyama, Takayuki Kobayashi, Atsushi Kohima, Koji Shinohara, Yoshiteru Sakamoto, Tsuguhiro Watanabi, Hitoshi Hojo and Tsuyoshi Imai, Plasma and Fusion Research **5** (2010), S2067.

[13] *Measurement of Ion Cyclotron Emissions by Using High-Frequency Magnetic Probes in the LHD*, Kenji Saito, Ryuhei Kumazawa, Tetsuo Seki, Hiroshi Kasahara, Goro Nomura, Fujio Shimpo, Hiroe Igami, Mitsutaka Isobe, Kunihiro Ogawa, Kazuo Toi, Masaki Osakabi Masaki Nishiura, Tsuguhiro Watanabi, Satoshi Yamamoto, Makoto Ichimura, Takashi Mutoh, Plasma Science and Technology **15** (2013), 209.

Core ICE

[14] *Ion cyclotron emission in NBI-heated plasmas in the TUMAN-3M tokamak*, L.G. Askinazi, A.A. Belokurov, D.B. Gin, V.A. kornev, S.V. Lebedev, A.E. Shevelev, A.S. Tukachinsky, N.A. Zhubr, Nucl. Fusion **58** (2018) 082003.

[15] *Alfvén Eigenmode and Energetic Particle Research in JT-60U*, H. Kimura, Y. Kusama, M. Saigusa, G.J. Kramer, K. Tobita, M. Nemoto, T. Konkoh, T. Nishitani, O. Da Costa, T. Ozeki, T. Oikawa, S. Moriyama, A. Morioka, G.Y. Fu, C. Z. Cheng, V. I. Afanastev, Nucl. Fusion **38** (1998), 1303.

[16] *Ion Cyclotron Emission on ASDEX Upgrade*, R. D'Inca, Ph.D thesis, Max Planck Institute for Plasma Physics, 2014.
(Yamamoto - IAEA)

Use of ICE measurements:

[17] *Ion cyclotron emission measurements during JET deuterium-tritium experiments*, G.A. Cottrell , V.P. Bhatnagar, O. Da Costa, R.O. Dendy, J. Jacquinot, K.G. McClements, D.C. McCune, M.F.F. Nave, P. Smeulders, D.F.H. Start, Nucl. Fusion **33** (1993) 1365.
[18] *Ion cyclotron emission from fusion-born ions in large tokamak plasmas: a brief review from JET and TFTR to ITER*, R O Dendy, K G McClements, Plasma Phys. and Control. Fusion **57** (2015) 044002.
[19] *Quantifying Fusion Born Ion Populations in Magnetically Confined Plasmas using Ion Cyclotron Emission*, L. Carbajal, R O Dendy S C Chapman, J W S Cook, Phys. Rev. Lett. **118** (2017) 105001.
[20] *Fast particle-driven ion cyclotron emission (ICE) in tokamak plasmas and the case for an ICE diagnostic in ITER,* K.G. McClements, R. D'Inca, R.O. Dendy, L. Carbaja, S.C. Chapman, J.W.S. Cook, R.W. Harvey, W.W. Heidbrink and S.D. Pinches, Nucl. Fusion **55** (2015) 043013.
[21] *Ion Cyclotron Emission Studies: Retrospects and Prospects*, N N Gorelenkov, Plasma Phys. Reports **42** (2016) 430.
[22] *Energetic particle-driven compressional Alfvén eigenmodes and prospects for ion cyclotron emission studies in fusion plasmas*, N N Gorelenkov, New J. Phys. **18** (2016) 105010.

Magneto-acoustic cyclotron instability:

[23] R. O. Dendy, C. N. Lashmore-Davies, and K. F. Kam, Phys. Fluids B **4** (1992), 3996.
[24] *The magnetoacoustic cyclotron instability of an extended shell distribution of energetic ions,* R. O. Dendy, C. N. Lashmore-Davies, and K. F. Kam, Phys. Fluids B **5** (1993), 1937.
[25] *The excitation of obliquely propagating fast Alfvén waves at fusion ion cyclotron harmonics,* R. O. Dendy, C. N. Lashmore-Davies, K. G. McClements, and G. A. Cottrell, Phys. Plasmas **1** (1994), 1918.
[26] *Alfvén Cyclotron Instability and Ion Cyclotron Emission,* Gorelenkov, N.N. and Cheng, C.Z., Nucl. Fusion **35** (1995) 1743.
[27] *Excitation of Alfvén cyclotron instability by charged fusion products in tokamaks*, N. N. Gorelenkov and C. Z. Cheng, Physics of Plasmas **2** (1995) 1961.
[28] *Interpretation of ion cyclotron emission from sub-Alfvénic fusion products in the Tokamak Fusion Test Reactor*, K G McClements, R O Dendy, C N Lashmore-Davier, G A Cottrell, Phys. Plasmas **3** (1996) 543.
[29] *Origin of Superthermal Ion Cyclotron emission in tokamaks*, T. Fülöp, Ya. I Kolesnichenko, M Lisak, D Anderson, Nucl. Fusion **37** (1997) 1281.
[30] *Ion cyclotron emission from fusion products and beam ions in the Tokamak Fusion Test Reactor*, T. Fülöp, M. Lisak, Nucl. Fusion **38** (1998) 761.

Other models

[31] *A mechanism for beam-driven excitation of ion cyclotron harmonic waves in the Tokamak Fusion Test Reactor,* R. O. Dendy, K. G. McClements, C. N. Lashmore-Davies, R. Majeski and S. Cauffman, Phys. Plasmas **1** (1994) 3407.
[32] *Ion cyclotron and spin-flip emissions from fusion products in tokamaks*, V. Arunasalam, G.J. Greene and K.M. Young, Nucl. Fusion **34** (1994) 927.

General CAE:

[33] *Physics of energetic particle-driven instabilities in the START spherical tokamak*, K G McClements, M P Gryaznevich, S E Sharapov, R J Akers, L C Appel, G F Counsel, C M Roach, R Majeski, Plasma Phys. Conrol. Fusion **41** (1999) 661.

[34] *Collective fast ion instability-induced losses in NSTX,* E.D. Fredrickson, R. Bell, D. Darrow, G. Fu, N. Gorelenkov, B. LeBlanc, S. Medley, J. Menard, H. Park, L. Roquemore, S. A. Sabbagh, D. Stutman, K. Tritz, N. Crocker, S. Kubota, W. Peebles, K.C. Lee, F. Levinton, Phys. of Plasmas **13** (2006) p056109.

[35] *Compressional Alfvén Eigenmodes on MAST*, L C Appel, T Fülöp, M J Hole, H M Smith, S D Pinches, R G L Vann, Plasma Phys. Control. Fusion **50** (2008) 115011.

[36] *Recent experiments on Alfvén eigenmodes in MAST*, M.P. Gryaznevich, S.E. Sharapov, M. Lilley, S.D. Pinches, A.R. Field, D. Howell, D. Keeling, R. Martin, H. Meyer, H. Smith, R. Vann, P. Denner, E. Verwichte and the MAST Team, Nucl. Fusion **48** (2008) 084003

[37] *Non-linear modulation of short wavelength compressional Alfvén eigenmodes*, E. D. Fredrickson, N. N. Gorelenkov, M. Podesta, A. Bortolon, N. A. Crocker, S. P. Gerhardt, R. E. Bell, A. Diallo, B. LeBlanc, F. M. Levinton, H. Yuh, Phys. of Plasmas **20**, 042112 (2013).

[38] *Internal amplitude, structure and identification of compressional and global Alfve ´n eigenmodes in NSTX*, N.A. Crocker, E.D. Fredrickson, N.N. Gorelenkov, W.A. Peebles, S. Kubota, R.E. Bell, A. Diallo, B.P. LeBlanc, J.E. Menard, M. Podesta`, K. Tritz, H. Yuh, Nucl. Fusion **53** (2013) 043017.

[39] *Bi-directional Alfvén cyclotron instabilities in the mega-amp spherical tokamak*, S. E. Sharapov, M. K. Lilley, R. Akers, N. Ben Ayed, M. Cecconello, J. W. S. Cook, G. Cunningham, E. Verwichte, and MAST Team, Phys. Plasmas **21** (2014), 082501

[40] *Compressional Alfvén eigenmodes in rotating spherical tokamak plasmas,* Håkan Smith, E D Fredrickson, Plasma Phys. Control. Fusion **59** (2017) 035007

ICE and CAE related:

[41] *Alfvén Cyclotron Instability and Ion Cyclotron Emission,* Gorelenkov, N.N. and Cheng, C.Z., Nucl. Fusion **35** (1995) 1743.

[42] *Excitation of Alfvén cyclotron instability by charged fusion products in tokamaks*, N. N. Gorelenkov and C. Z. Cheng, Physics of Plasmas **2** (1995) 1961.

[43] M. Ono, S. M. Kaye, Y.-K. M. Peng, G. Barnes, W. Blanchard, M. D. Carter, J. Chrzanowski, L. Dudek, R. Ewig, D. Gates, R. E. Hatcher, T. Jarboe, S. C. Jardin, D. Johnson, R. Kaita, M. Kalish, C. E. Kessel, H. W. Kugel, R. Maingi, R. Majeski, J. Manickam, B. McCormack, J. Menard, D. Mueller, B. A. Nelson, B. E. Nelson, C. Neumeyer, G. Oliaro, F. Paoletti, R. Parsells, E. Perry, N. Pomphrey, S. Ramakrishnan, R. Raman, G. Rewoldt, J. Robinson, A. L. Roquemore, P. Ryan, S. Sabbagh, D. Swain, E. J. Synakowski, M. Viola, M. Williams, J. R. Wilson, and NSTX Team, Nucl. Fusion **40**, 557 (2000).

[44] M. Ono, J. Chryzanowski, L. Dudek, *et al*., Nucl. Fusion **55** (2015) 073007.